

1           **Adsorption characteristics of bovine serum albumin onto alumina with a specific**  
2  
3           **crystalline structure**

4  
5  
6           Masakazu Kawashita<sup>a,\*</sup>, Junpei Hayashi<sup>a</sup>, Zhixia Li<sup>b</sup>, Toshiki Miyazaki<sup>c</sup>, Masami Hashimoto<sup>d</sup>,  
7           Hiroki Hihara<sup>e</sup> and Hiroyasu Kanetaka<sup>e</sup>

8  
9  
10  
11           <sup>a</sup>Graduate School of Biomedical Engineering, Tohoku University, Sendai 980-8579, Japan

12  
13           <sup>b</sup>College of Chemistry and Chemical Engineering, Guangxi University, Nanning 530004,  
14  
15           China

16  
17           <sup>c</sup>Graduate School of Life Science and Systems Engineering, Kyushu Institute of Technology,  
18           Kitakyushu 808-0196, Japan

19  
20           <sup>d</sup>Japan Fine Ceramics Center, Nagoya 456-8587, Japan

21  
22           <sup>e</sup>Graduate School of Dentistry, Tohoku University, Sendai 980-8575, Japan

23  
24  
25  
26  
27           \* Corresponding author. Tel.: +81 227953937. fax: +81 227954735

28  
29           E-mail address: m-kawa@ecei.tohoku.ac.jp (M. Kawashita).

1 **Abstract**

2 Bone cement containing alumina particles with a specific crystalline structure  
3 exhibits the ability to bond with bone. These particles (AL-P) are mainly composed of  
4 delta-type alumina ( $\delta\text{-Al}_2\text{O}_3$ ). It is likely than some of the proteins present in the body  
5 environment are adsorbed onto the cement and influence the expression of its bioactivity.  
6 However, the effect that this adsorption of proteins has on the bone-bonding mechanism of  
7 bone cement has not yet been studied. In this study, we investigated the characteristics of the  
8 adsorption of bovine serum albumin (BSA) onto AL-P and compared them with those of its  
9 adsorption onto hydroxyapatite (HA), which also exhibits bone-bonding ability, and with  
10 those onto alpha-type alumina ( $\alpha\text{-Al}_2\text{O}_3$ ), which does not bond with bone. The adsorption  
11 characteristics of BSA onto AL-P were very different from those onto  $\alpha\text{-Al}_2\text{O}_3$  but quite  
12 similar to those onto HA. It is speculated that BSA is adsorbed onto AL-P and HA by  
13 interionic interactions, while it is adsorbed onto  $\alpha\text{-Al}_2\text{O}_3$  by electrostatic attraction. The  
14 results suggest that the specific adsorption of albumin onto implant materials might play a  
15 role in the expression of the bone-bonding abilities of the materials.  
16  
17  
18  
19  
20  
21  
22  
23  
24  
25  
26

27 **Keywords:**  $\delta\text{-Al}_2\text{O}_3$ ,  $\alpha\text{-Al}_2\text{O}_3$ , hydroxyapatite, albumin, adsorption  
28  
29  
30  
31  
32  
33  
34  
35  
36  
37  
38  
39  
40  
41  
42  
43  
44  
45  
46  
47  
48  
49  
50  
51  
52  
53  
54  
55  
56  
57  
58  
59  
60  
61  
62  
63  
64  
65

## 1. Introduction

Most artificial materials with the ability to bond with bone form an apatite layer on their surfaces and bond to living bone through this apatite layer [1,2]. This means artificial materials with the ability to form apatite in the body environment have the potential to bond to living bone. In 1990, Kokubo and colleagues showed that structural changes that take place *in vivo* on the surfaces of bioactive glass-ceramics can be reproduced in an acellular simulated body fluid (SBF) with ion concentrations nearly similar to those of human blood plasma [3]. This SBF does not contain any cells and proteins and can be prepared by simply dissolving the chemical reagents in pure water in the correct proportions [4]. Therefore, it has come to be widely used for the evaluation of the apatite-forming abilities of artificial materials.

Even though the SBF is useful for evaluating the apatite-forming abilities of materials, inconsistencies have been reported in the apatite-forming abilities determined using SBF and the *in vivo* bone-bonding abilities of the materials. For example, abalone shell forms apatite in SBF [5], but does not bond to living bone [6]. In contrast,  $\beta$ -tricalcium phosphate ( $\beta$ -TCP) does not form apatite in SBF [7], but bonds to living bone [8]. Similar inconsistencies were also observed in the case of bone cement containing alumina particles with a specific crystalline structure [9-12]. The particles (AL-P) are mainly composed of delta-type alumina ( $\delta$ - $\text{Al}_2\text{O}_3$ ). These results suggest that proteins and/or cells that are not present in the SBF play a role in the expression of the bone-bonding ability of materials. It was confirmed that the osteoblastic differentiation of bone marrow cells was more effective on a bone cement containing AL-P than on a resin containing alpha type-alumina ( $\alpha$ - $\text{Al}_2\text{O}_3$ ) particles [13]; however, the effects of the adsorption of proteins on the bone-bonding mechanism have not yet been investigated. It is assumed that bone bonding progresses in six stages: (1) serum protein adsorption, (2) cell recruitment, (3) cell attachment and proliferation, (4) cell differentiation and activation (5) matrix calcification, and finally (6) bone remodeling [14,15]. Therefore, immediately after the biomaterial has been implanted, it is coated by an adsorbed layer of proteins present in blood and tissue fluids, and the subsequent cellular responses are dependent on these proteins adsorbed onto the surface of the implant. This is

1 particularly true during the early stage of the implant-cell interaction [16,17].

2  
3 Of the numerous kinds of proteins found in human blood plasma, in this study, we  
4 focused on albumin, because albumin is an abundant and multifunctional protein [18], and  
5 hence, we speculate that the albumin adsorbed onto the surface of the implant affects the  
6 initial cell response [19]. Also, our recent study investigating the adsorption of bovine serum  
7 albumin (BSA) onto hydroxyapatite (HA), which exhibits bone-bonding ability, as well as  
8 onto  $\alpha$ -Al<sub>2</sub>O<sub>3</sub>, which does not, had shown that the specific adsorption of albumin onto HA  
9 probably influences the adhesion and proliferation of osteoblasts [20,21]. Therefore, in this  
10 study, we hypothesized that BSA would adsorb specifically onto AL-P as was the case for HA,  
11 and investigated the adsorption behavior of BSA onto bioactive AL-P, comparing it with those  
12 in the cases of HA and  $\alpha$ -Al<sub>2</sub>O<sub>3</sub>.  
13  
14  
15  
16  
17  
18  
19  
20  
21  
22  
23  
24  
25

## 26 **2. Materials and methods**

### 27 2.1. Structural analyses of the tested materials

28  
29 The alumina particles (AL-P) used were prepared by the fusion and subsequent  
30 quenching of  $\alpha$ -Al<sub>2</sub>O<sub>3</sub> [9-13]. The HA (HAP-200, Taihei Chemical Industrial Co. Ltd., Osaka,  
31 Japan) and  $\alpha$ -Al<sub>2</sub>O<sub>3</sub> powders (ALO14PB, Kojundo Chemical Lab. Co. Ltd., Saitama, Japan)  
32 used were obtained commercially. The crystalline phases of the tested materials were  
33 examined using powder X-ray diffraction (XRD) analyses (RINT-2200VL, Rigaku Co. Ltd.,  
34 Tokyo, Japan), which were performed using an X-ray source that emitted Ni-filtered CuK $\alpha$   
35 radiation. The X-ray power used was 40 kV and the current used was 40 mA. The scanning  
36 rate was 2°/min and the sampling angle was 0.02°. The sizes and shapes of the tested  
37 materials were determined using scanning electron microscopy (SEM) (VE-8800, Keyence,  
38 Tokyo, Japan). The specific surface areas (SSAs) of the samples were determined via nitrogen  
39 adsorption, measured using the Brunauer-Emmett-Teller (BET) technique (Autosorb-iQ,  
40 Quantachrome Instruments, Florida, USA).  
41  
42  
43  
44  
45  
46  
47  
48  
49  
50  
51  
52  
53  
54  
55  
56  
57

### 58 2.2 Measurement of the zeta potentials of the tested materials

1 The zeta-potentials of the tested materials and of BSA solutions in saline with pH  
2 values ranging from 4.0 to 7.4 were measured using laser electrophoresis spectroscopy  
3 (ELS-Z) (Otsuka Electronics Co. Ltd., Osaka, Japan and Zetasizer Nano ZS90, Malvern  
4 Instruments Ltd., Worcestershire, UK). The pH was controlled using 10 mM solutions of  
5 NaOH or HCl.  
6  
7  
8  
9

### 10 11 12 13 2.3. Measurement of BSA adsorption onto the particles of the tested materials 14 15

16 Commercially available BSA (Jackson ImmunoResearch Laboratories Inc.,  
17 Pennsylvania, USA) was dissolved in saline to obtain BSA solutions having concentrations  
18 ranging from 0.3 to 1.0 mg/ml. 100 mg of AL-P was soaked in 0.15 ml of each of the BSA  
19 solutions in microtubes (GDMSR-2ML, As One Corp., Osaka, Japan); 18 mg of the HA  
20 powder was soaked in 1.2 ml of each of the BSA solutions in microtubes; and finally, 100 mg  
21 of the  $\alpha$ -Al<sub>2</sub>O<sub>3</sub> powder were soaked in 5 ml of each of the BSA solutions in centrifuge tubes  
22 (CN-1050, As One Corp., Osaka, Japan). The BSA solutions were then vortexed for 10 s and  
23 the tubes containing them were rotated at 20 rpm at 36.5°C for 1 h using a tube rotator  
24 (TR-350, As One Corp., Osaka, Japan). The mixtures were then centrifuged for 5 min at 6000  
25 rpm, and the protein concentrations of the supernatants were determined using the Bradford  
26 dye binding assay [22]. A microplate reader (Sunrise Remote CTR-S, Tecan Japan Co., Ltd.,  
27 Kanagawa, Japan) was employed for the process. The adsorption of BSA onto the particles of  
28 the tested materials was also investigated using saline solutions having pH values of 4.0, 5.5,  
29 and 7.4. A control experiment was performed using the BSA solutions of different  
30 concentrations to determine the loss in protein in the absence of soaked samples. It was found  
31 that the protein concentrations changed by less than 10% in the absences of soaked samples.  
32 Ten samples of each material were tested for BSA adsorption.  
33  
34  
35  
36  
37  
38  
39  
40  
41  
42  
43  
44  
45  
46  
47  
48  
49  
50  
51  
52  
53

### 54 2.4. Limited proteolysis of the BSA adsorbed onto the particles of the tested materials 55

56 20 mg of AL-P, 15 mg of HA, and 20 mg of  $\alpha$ -Al<sub>2</sub>O<sub>3</sub> each were soaked in 1 ml of the  
57 BSA solution with a concentration of 0.4 mg/ml. The resulting BSA solutions containing the  
58  
59  
60

1 tested materials were then rotated at 20 rpm at 36.5°C for 1 h using a tube rotator. 50 µl of  
2 each BSA solution was then centrifuged for 1 min. (CF15RXII, Hitachi, Tokyo, Japan). The  
3 supernatants were removed using a micropipette, and 500 µl of a 20 mmol/l Tris-HCl buffer  
4 was added to the sediments. Then, the solutions were again centrifuged for 1 min. and the  
5 supernatants were subsequently removed again. 50 µl of 20 mmol/l Tris-HCl buffer was  
6 added again to the sediments and the resulting solutions vortexed for 10 s. Then, 2 µl of  
7 trypsin (T6567-5X20UG, Sigma-Aldrich Co., Missouri, USA) was added to the solutions,  
8 which were left undisturbed for 1 min. Next, 10 µl of Tris buffer was added to each of the  
9 solutions, and the solutions were heated at 100°C for 5 min.

## 21 2.5. Sodium dodecyl sulfate–polyacrylamide gel electrophoresis (SDS-PAGE)-based analyses 22 of the fragments of BSA adsorbed onto the particles of the tested materials

23 A sodium dodecyl sulfate (SDS) buffer and a precast gel (HOG-0520-17, Oriental  
24 Instruments Co. Ltd., Kanagawa, Japan) were set in an electrophoresis tank (DPE-1020,  
25 Cosmo Bio Co., Ltd., Tokyo, Japan). 10 µl of the sample solution being tested and 10 µl of a  
26 BenchMark™ prestained protein ladder (10748-010, Life Technologies Corporation, California,  
27 USA) were placed in the well of the tank and electrophoresed at 30 mA for 1 h.  
28 Post-electrophoresis, the gel was soaked in a Coomassie brilliant blue (CBB) solution  
29 (7664-38-2, Bio-Rad Laboratories, Inc., California, USA) and shaken for 2 min using a “Belly  
30 Dancer” shaker (CMBAA115S, Stovall Life Science Inc., North Carolina, USA). The gel was  
31 then soaked in a decolorizing solution and shaken again for 30 min using the Belly Dancer  
32 shaker.

## 3. Results and discussion

33 Figure 1 shows the XRD patterns of (a) AL-P, (b) the HA powder, and (c) the  
34  $\alpha$ -Al<sub>2</sub>O<sub>3</sub> powder. Several high-intensity peaks ascribable to  $\delta$ -Al<sub>2</sub>O<sub>3</sub> (PDF#46-1131) and as  
35 well as low-intensity ones attributable to  $\alpha$ -Al<sub>2</sub>O<sub>3</sub> (PDF#42-1468) and  $\gamma$ -Al<sub>2</sub>O<sub>3</sub>  
36 (PDF#10-0425) were observed in the case of AL-P. These indicated that the AL-P used was

1 mainly composed of  $\delta$ -Al<sub>2</sub>O<sub>3</sub> but contained small amounts of  $\alpha$ -Al<sub>2</sub>O<sub>3</sub> and  $\gamma$ -Al<sub>2</sub>O<sub>3</sub>. The XRD  
2 patterns of the HA and  $\alpha$ -Al<sub>2</sub>O<sub>3</sub> powders used in this study exhibited diffraction peaks  
3 ascribable to hydroxyapatite (PDF#09-0432) and  $\alpha$ -Al<sub>2</sub>O<sub>3</sub> (PDF#42-1468), respectively.  
4

5  
6  
7 Figure 2 shows SEM images of (a) AL-P, (b) the HA powder, and (c) the  $\alpha$ -Al<sub>2</sub>O<sub>3</sub>  
8 powder. The insets show magnified images of the corresponding materials. In the case of  
9 AL-P, the primary particles had smooth surfaces, were 2–10  $\mu$ m in diameter, and formed  
10 aggregates around 20  $\mu$ m in size. The HA and  $\alpha$ -Al<sub>2</sub>O<sub>3</sub> powders were also composed of very  
11 fine particles that formed agglomerates and short chains. The agglomerates of HA and  
12  $\alpha$ -Al<sub>2</sub>O<sub>3</sub> had sizes ranging from 5 to 20  $\mu$ m and from 1 to 20  $\mu$ m, respectively. The results of  
13 the BET measurements showed that the SSAs of AL-P, the HA powder, and the  $\alpha$ -Al<sub>2</sub>O<sub>3</sub>  
14 powder were 0.759, 9.345, and 1.685 m<sup>2</sup>/g, respectively. Although the sizes of the aggregates  
15 of all the tested materials were almost the same, AL-P had a lower SSA than those of the HA  
16 and  $\alpha$ -Al<sub>2</sub>O<sub>3</sub> powders. This was because the surface of AL-P was denser than those of the HA  
17 and  $\alpha$ -Al<sub>2</sub>O<sub>3</sub> powders, as can be seen from the magnified SEM images in Fig. 2.  
18  
19  
20  
21  
22  
23  
24  
25  
26  
27  
28  
29

30 Figure 3 shows the zeta potentials of AL-P, the HA powder, and the  $\alpha$ -Al<sub>2</sub>O<sub>3</sub> powder.  
31 AL-P exhibited a positive zeta potential at pH of 4.0 but exhibited negative ones at pH values  
32 of 5.5 and 7.4. The results were the same for HA in BSA. In contrast, the  $\alpha$ -Al<sub>2</sub>O<sub>3</sub> powder  
33 exhibited only positive zeta potentials over the examined range of pH values. We had  
34 previously found that  $\delta$ -Al<sub>2</sub>O<sub>3</sub> derived from the heat treatment of boehmite tended to exhibit  
35 negative zeta potentials in SBF, whereas other phases such as  $\gamma$ -Al<sub>2</sub>O<sub>3</sub> or  $\theta$ -Al<sub>2</sub>O<sub>3</sub> exhibited  
36 positive ones [23]. It was difficult to interpret the present results on the basis of those of our  
37 previous study because the electrolytes used for the zeta potential measurements in the two  
38 studies were different. However, we can speculate that  $\delta$ -Al<sub>2</sub>O<sub>3</sub>, the dominant crystalline  
39 phase of AL-P, contributes to the negative zeta potentials noticed in the case of AL-P at pH  
40 values of 5.5 and 7.4.  
41  
42  
43  
44  
45  
46  
47  
48  
49  
50  
51  
52

53 Figure 4 shows the isotherms for the adsorption of BSA onto the particles of AL-P,  
54 those of the HA powder, and those of the  $\alpha$ -Al<sub>2</sub>O<sub>3</sub> powder. Figure 5 shows the adsorption data  
55 plotted in the form of  $C/q$  versus  $C$  curves, with the results of the linear regression analyses of  
56  
57  
58  
59  
60  
61  
62  
63  
64  
65

1 the data also shown. Here,  $C$ ,  $q$ , and  $R^2$  are the concentration of the BSA solution tested, the  
2 amount of BSA adsorbed, and the square of the correlation coefficient, respectively. The  
3 isotherms for the adsorption of BSA onto the tested materials were similar to Langmuir-type  
4 isotherms, indicating that the adsorption was of the chemisorption type and took place via the  
5 formation of monolayers. In addition, the coefficients of determination ( $R^2$ ) for AL-P (0.9758)  
6 and HA (0.9739) were almost similar (see Fig. 5), suggesting that the mechanism for the  
7 adsorption of BSA onto AL-P was similar to that for its adsorption onto HA.  
8

9  
10  
11  
12  
13  
14  
15  
16  
17  
18  
19  
20  
21  
22  
23  
24  
25  
26  
27  
28  
29  
30  
31  
32  
33  
34  
35  
36  
37  
38  
39  
40  
41  
42  
43  
44  
45  
46  
47  
48  
49  
50  
51  
52  
53  
54  
55  
56  
57  
58  
59  
60  
61  
62  
63  
64  
65

Figure 6 shows the adsorption capacity of BSA onto AL-P and those onto the HA and  $\alpha$ - $\text{Al}_2\text{O}_3$  powders for different pH values. Over the investigated pH range, the adsorption capacity of BSA onto  $\alpha$ - $\text{Al}_2\text{O}_3$  was greater than those on HA or AL-P. This might be owing to the electrostatic interaction between BSA and  $\alpha$ - $\text{Al}_2\text{O}_3$  [20]. As shown in Fig. 3, BSA, HA, and AL-P exhibited negative zeta potentials whereas  $\alpha$ - $\text{Al}_2\text{O}_3$  showed a positive one at pH values of 5.5 and 7.4. It is likely that this results in electrostatic attraction between BSA and  $\alpha$ - $\text{Al}_2\text{O}_3$  and electrostatic repulsion between BSA and HA and between BSA and AL-P. Thus, as a result,  $\alpha$ - $\text{Al}_2\text{O}_3$  had a larger binding capacity with respect to BSA than did HA or AL-P. It should be noted that  $\alpha$ - $\text{Al}_2\text{O}_3$  had a greater binding capacity with respect to BSA than did HA or AL-P even when the pH was 4.0. This was in spite of the positive zeta potentials of both BSA and  $\alpha$ - $\text{Al}_2\text{O}_3$  (see Fig. 3). The reason for this phenomenon is unclear, but the positive zeta potentials of both BSA and  $\alpha$ - $\text{Al}_2\text{O}_3$  might partly be responsible for the adsorption capacity of BSA onto  $\alpha$ - $\text{Al}_2\text{O}_3$  being greater even at pH 4.0. It should also be noted that both HA and AL-P exhibited nonzero binding capacities with respect to BSA despite the electrostatic repulsion between them and BSA. This implies that other forces of attraction such as local ionic interactions between BSA and the specific adsorption sites on the particles of these materials (i.e., HA and AL-P) should also be considered. As can be seen from Fig. 6, the adsorption capacity of BSA onto HA decreased gradually with an increase in the pH value. This might have been because the specific adsorption sites on the HA particles, presumably present in the form of positively charged calcium ions on the  $a$ -face [24,25], were terminated by hydroxyl ( $\text{OH}^-$ ) ions as the pH was increased. Further, the adsorption capacity



1 of BSA onto AL-P also decreased gradually with an increase in the pH. This result suggested  
2 that AL-P also has specific adsorption sites and that the mechanism for the adsorption of BSA  
3 onto AL-P is similar to that for its adsorption onto HA as indicated in Fig. 5. Here, we have  
4 much concern about the relationship between BSA adsorption characteristics and  
5 bone-bonding ability of the materials. Further study is still needed to clarify the relationship,  
6 but our recent study [26] suggested that BSA adsorbed on HA stimulates a different cell  
7 response than  $\alpha$ -Al<sub>2</sub>O<sub>3</sub> and that quick adherence of osteoblast cells and  
8 monocyte-macrophage lineage cells plays a role in HA osteoconductivity.

17 Figure 7 shows the results of the SDS-PAGE analyses of fragments of BSA adsorbed  
18 on (a) AL-P, (b) the HA powder, and (c) the  $\alpha$ -Al<sub>2</sub>O<sub>3</sub> powder. Interestingly, both AL-P and HA  
19 resulted in a single band at a molecular mass of approximately 70 kDa, whereas  $\alpha$ -Al<sub>2</sub>O<sub>3</sub>  
20 resulted in three bands, at molecular masses of approximately 35 kDa, 55 kDa, and 70 kDa,  
21 respectively. The band at approximately 70 kDa was attributable to BSA fragments produced  
22 by proteolysis near the terminal such as K(3) or K(593) etc. and/or to BSA molecules  
23 themselves that might have been desorbed from the sample particles into the sample buffer  
24 prior to electrophoresis. Given the primary structure of BSA [27] and the active sites of BSA  
25 for trypsin, the BSA fragments with molecular masses of approximately 35 and 55 kDa are  
26 listed in Table 1. It is difficult to identify the BSA fragments more specifically at this moment,  
27 but it is believed that the state in which BSA is adsorbed onto AL-P is much different from  
28 that in which it is adsorbed onto  $\alpha$ -Al<sub>2</sub>O<sub>3</sub> and similar to that in which it is adsorbed onto HA.

42 Next, we discuss the mechanism by which BSA is adsorbed onto AL-P. It has been  
43 reported that  $\delta$ -Al<sub>2</sub>O<sub>3</sub> and  $\gamma$ -Al<sub>2</sub>O<sub>3</sub> have positively charged Lewis acid sites [28], which are  
44 formed by the partial dehydration of the OH group on  $\delta$ -Al<sub>2</sub>O<sub>3</sub> and  $\gamma$ -Al<sub>2</sub>O<sub>3</sub> by heating [29].  
45 Hence, the AL-P used in this study might also have similar positively charged Lewis acid sites.  
46 On the other hand, BSA has negatively charged COO<sup>-</sup> sites on its aspartic acid and glutamic  
47 acid residues [27]. Therefore, we speculate that BSA is adsorbed onto AL-P by interionic  
48 interactions between the positively charged Lewis acid sites of AL-P and the negatively  
49 charged COO<sup>-</sup> sites of BSA (see Fig. 8). Similar interionic interactions might be responsible  
50

1 for the adsorption of BSA onto HA, because HA has positively charged calcium ions on the  
2 *a*-face [24,25]. As a result, the characteristics of the adsorption of BSA onto AL-P were  
3 similar to those onto HA, as shown in Figs. 4–7. In contrast,  $\alpha$ -Al<sub>2</sub>O<sub>3</sub> does not have such  
4 specific Lewis acid sites, and hence, BSA is adsorbed onto  $\alpha$ -Al<sub>2</sub>O<sub>3</sub> mainly owing to  
5 electrostatic attraction. In fact, BSA was adsorbed onto  $\alpha$ -Al<sub>2</sub>O<sub>3</sub> in much larger amounts when  
6 the surface charge of  $\alpha$ -Al<sub>2</sub>O<sub>3</sub> was opposite to that of BSA (see Figs. 3 and 6). The detailed  
7 mechanism of BSA adsorption still not be fully clarified in this study, but the above  
8 speculation might contribute to understanding of the adsorption mechanism.

9  
10  
11  
12  
13  
14  
15  
16  
17 In conclusion, the present results demonstrate that the characteristics of the  
18 adsorption of BSA onto AL-P are much different from those of its adsorption onto  $\alpha$ -Al<sub>2</sub>O<sub>3</sub>  
19 but quite similar to those of its adsorption onto HA. These results partly supported our  
20 hypothesis that the specific adsorption of albumin onto implant materials plays a role in the  
21 expression of the bone-bonding abilities of the materials.

#### 22 23 24 25 26 27 28 29 30 **4. Conclusions**

31  
32 We investigated the characteristics of the adsorption of BSA onto AL-P and  
33 compared them with those of its adsorption onto HA and  $\alpha$ -Al<sub>2</sub>O<sub>3</sub>. We found that the  
34 characteristic of the adsorption of BSA onto AL-P were much different from those onto  
35  $\alpha$ -Al<sub>2</sub>O<sub>3</sub> and similar to those onto HA. It is speculated that BSA adsorbs onto AL-P and HA  
36 via interionic interactions, while it is adsorbed onto  $\alpha$ -Al<sub>2</sub>O<sub>3</sub> by electrostatic attraction. The  
37 present results imply that specific adsorption of albumin onto implant materials might affect  
38 expression of the bone-bonding abilities of the materials.

#### 39 40 41 42 43 44 45 46 47 48 49 **Acknowledgements**

50  
51 This work was partially supported by a research grant from the Inamori Foundation,  
52 Japan and a Grant-in-Aid for Scientific Research from The Ministry of Education, Culture,  
53 Sports, Science and Technology, Japan. The authors thank Mr. Okano and Mr. Kaji, Taihei  
54 Chemical Industrial Co. Ltd., for providing the HA powder. They also thank Prof. Ishida,  
55  
56  
57  
58  
59  
60  
61  
62  
63  
64  
65

1 Tohoku University, and Dr. Maeda, Nagoya Institute of Technology, for the use of the  
2 instrument to measure the specific surface areas.  
3  
4  
5

## 6 **References**

- 7  
8  
9 1. Hench LL, Splinger RJ, Allen WC, Greenlee TK. Bonding mechanisms at the interface of  
10 ceramic prosthetic materials. *J Biomed Mater Res* 1972;2:117-141.
- 11  
12 2. Kokubo T, Shigematsu M, Nagashima Y, Tashiro M, Nakamura T, Yamamuro T, Higashi  
13 S. Apatite- and wollastonite-containing glass-ceramics for prosthetic application. *Bull*  
14 *Inst Chem Res Kyoto Univ* 1982;60:260-268.
- 15  
16 3. Kokubo T, Kushitani H, Sakka S, Kitsugi T, Yamamuro T. Solutions able to reproduce in  
17 vivo surface-structure changes in bioactive glass-ceramic A-W *J Biomed Mater Res*  
18 1990;24:721-734.
- 19  
20 4. Kokubo T, Takadama H. How useful is SBF in predicting in vivo bone bioactivity?  
21 *Biomater* 2006;27:2907-2915.
- 22  
23 5. Ohtsuki C, Aoki Y, Kokubo T, Fujita Y, Kotani S, Yamamuro T. Bioactivity of limestone  
24 and abalone shell. In: *Transactions of the 11th Annual Meeting of Japanese Society for*  
25 *Biomaterials*. 1989. p. 12.
- 26  
27 6. Fujita Y, Yamamuro T, Nakamura T, Kotani S, Kokubo T, Ohtsuki C. The bonding  
28 behavior of limestone and abalone shell to bone. In: *Transactions of the 11th Annual*  
29 *Meeting of Japanese Society for Biomaterials*. 1989. p. 3.
- 30  
31 7. Ohtsuki C, Kokubo T, Neo M, Kotani S, Yamamuro T, Nakamura T, Bando Y.  
32 Bone-bonding mechanism of sintered beta-3CaO·P<sub>2</sub>O<sub>5</sub>. *Phosphorus Res Bull*  
33 1991;1:191-196.
- 34  
35 8. Kotani S, Fujita Y, Kitsugi T, Nakamura T, Yamamuro T, Ohtsuki C, Kokubo T. Bone  
36 bonding mechanism of  $\beta$ -tricalcium phosphate. *J Biomed Mater Res* 1991;25:1303-1315.
- 37  
38 9. Kobayashi M, Kikutani T, Kokubo T, Nakamura T. Direct bone formation on alumina  
39 bead composite. *J Biomed Mater Res* 1997;37:555-565.
- 40  
41 10. Okada K, Kobayashi M, Neo M, Shinzato S, Matsushita M, Kokubo T, Nakamura T.  
42  
43  
44  
45  
46  
47  
48  
49  
50  
51  
52  
53  
54  
55  
56  
57  
58  
59  
60  
61  
62  
63  
64  
65

- 1 Ultrastructure of the interface between alumina bead composite and bone. *J Biomed*  
2 *Mater Res* 2000;49:106-111.
- 3
- 4
- 5 11. Shinzato S, Kobayashi M, Choju K, Kokubo T, Nakamura T. Bone-bonding behavior of  
6 alumina bead composite. *J Biomed Mater Res* 1999;49:287-300.
- 7
- 8
- 9 12. Shinzato S, Nakamura T, Kokubo T, Kitamura Y. Composites consisting of poly(methyl  
10 methacrylate) and alumina powder: an evaluation of their mechanical and biological  
11 properties. *J Biomed Mater Res* 2002;60:585-591.
- 12
- 13
- 14
- 15 13. Nishio K, Neo M, Akiyama H, Okada Y, Kokubo T, Nakamura T. Effects of apatite and  
16 wollastonite containing glass-ceramic powder and two types of alumina powder in  
17 composites on osteoblastic differentiation of bone marrow cells. *J Biomed Mater Res*  
18 2001;55:164-176.
- 19
- 20
- 21
- 22
- 23
- 24 14. Puleo DA, Nanci A. Understanding and controlling the bone-implant interface. *Biomater*  
25 1999;20:2311-2321.
- 26
- 27
- 28 15. Nakamura M, Sekijima Y, Nakamura S, Kobayashi T, Niwa K, Yamashita K. Role of  
29 blood coagulation components as intermediators of high osteoconductivity of electrically  
30 polarized hydroxyapatite. *J Biomed Mater Res A* 2006;79:627-634.
- 31
- 32
- 33
- 34 16. Castner DG, Ratner BD. Biomedical surface science: foundations to frontiers. *Surf Sci*  
35 2002;500:28-60.
- 36
- 37
- 38
- 39 17. Tirrell M, Kokkoli E, Biesalski M. The role of surface science in bioengineered materials.  
40 *Surf Sci* 2002;500:61-83.
- 41
- 42
- 43 18. Curry S, Brick P, Franks NP. Fatty acid binding to human serum albumin: new insights  
44 from crystallographic studies. *Biochim Biophys Acta* 1999;1441:131-140.
- 45
- 46
- 47 19. Pitt WG, Park K, Cooper SL. Sequential protein adsorption and thrombus deposition on  
48 polymeric biomaterials. *J Colloid Interf Sci* 1986;111: 343-362.
- 49
- 50
- 51 20. Hayashi J, Kawashita M, Miyazaki T, Kamitakahara M, Ioku K, Kanetaka H. Comparison  
52 of adsorption behavior of bovine serum albumin and osteopontin on hydroxyapatite and  
53 alumina. *Phosphorus Res Bull* 2012;26:23-28.
- 54
- 55
- 56
- 57 21. Hayashi J, Kawashita M, Miyazaki T, Kudo T, Kanetaka H, Hashimoto M. MC3T3-E1
- 58
- 59
- 60
- 61
- 62
- 63
- 64
- 65

- 1 cell response to hydroxyapatite and alpha-type alumina adsorbed with bovine serum  
2 albumin. Key Eng Mater 2013;529-530:365-369  
3  
4  
5 22. Bradford MM. A rapid and sensitive method for the quantitation of microgram quantities  
6 of protein utilizing the principle of protein-dye binding. Anal Biochem 1976;72:248-254.  
7  
8  
9 23. Kawashita M, Kamitani A, Miyazaki T, Matsui N, Li Z, Kanetaka H, Hashimoto M. Zeta  
10 potential of alumina powders with different crystalline phases in simulated body fluid.  
11 Mater Sci Eng C 2012;32:2617-2622.  
12  
13  
14  
15 24. Kawasaki T, Takahashi S, Ikeda K. Hydroxyapatite high-performance liquid  
16 chromatography: column performance for proteins. Eur J Biochem 1985;152:361-371.  
17  
18  
19 25. Kawasaki T, Ikeda K, Takahashi S, Kuboki Y. Further study of hydroxyapatite  
20 high-performance liquid chromatography using both proteins and nucleic acids, and a  
21 new technique to increase chromatographic efficiency. Eur J Biochem 1986;155:249-257.  
22  
23  
24  
25  
26 26. Kawashita M, Hayashi J, Kudo T, Kanetaka H, Li Z, Miyazaki T, Hashimoto M.  
27 MC3T3-E1 and RAW264.7 cell response to hydroxyapatite and alpha-type alumina  
28 adsorbed with bovine serum albumin. J Biomed Mater Res Part A, in press.  
29  
30  
31  
32 27. Hirayama K, Akashi S, Furuya M, Fukuhara K. Rapid confirmation and revision of the  
33 primary structure of bovine serum albumin by ESIMS and FRIT-FAB LC/MS. Biochem  
34 Biophys Res Comm 1990;173:639-646.  
35  
36  
37  
38 28. Metivier R, Leray I, Lefevre JP, Auberger MR, Szydliwski NZ, Valeur B.  
39 Characterization of alumina surfaces by fluorescence spectroscopy. Phys Chem  
40 2003;5:758-766.  
41  
42  
43  
44  
45 29. Wischert R, Laurent P, Coperet C, Delbecq F, Sautet P.  $\gamma$ -Alumina: the essential and  
46 unexpected role of water for the structure, stability, and reactivity of “defect” sites. J Am  
47 Chem Soc 2012;134:14430-14449.  
48  
49  
50  
51  
52  
53  
54  
55  
56  
57  
58  
59  
60  
61  
62  
63  
64  
65

1  
2  
3 **Figure and table captions**

4  
5 Figure 1 X-ray diffraction (XRD) patterns of (a) AL-P, (b) the HA powder, and (c) the  
6  $\alpha$ -Al<sub>2</sub>O<sub>3</sub> powder.  
7

8  
9 Figure 2 Scanning electron microscopic (SEM) images of (a) AL-P, (b) the HA powder, and  
10 (c) the  $\alpha$ -Al<sub>2</sub>O<sub>3</sub> powder. The insets show magnified images.  
11

12  
13 Figure 3 Zeta potentials of AL-P and of the HA and  $\alpha$ -Al<sub>2</sub>O<sub>3</sub> powders.  
14

15  
16 Figure 4 Isotherms for the adsorption of BSA onto AL-P and onto the HA and  $\alpha$ -Al<sub>2</sub>O<sub>3</sub>  
17 powders.  
18

19  
20 Figure 5 The adsorption data plotted in the form of  $C/q$  versus  $C$  curves and the results of  
21 the linear regression analyses of the curves ( $C$ : BSA solution concentration;  $q$ : the  
22 amount of BSA adsorbed; and  $R^2$ : the square of the correlation coefficient).  
23

24  
25 Figure 6 Characteristics of the adsorption of BSA onto AL-P and onto the HA and  $\alpha$ -Al<sub>2</sub>O<sub>3</sub>  
26 powders at different pH values.  
27

28  
29 Figure 7 SDS-PAGE analysis of the fragments of BSA adsorbed onto (a) AL-P, (b) the HA  
30 powder, and (c) the  $\alpha$ -Al<sub>2</sub>O<sub>3</sub> powder.  
31

32  
33 Figure 8 Possible mechanisms for the specific adsorption of BSA onto AL-P and onto HA.  
34

35  
36  
37  
38 Table 1 BSA fragments with molecular masses of approximately 35 and 55 kDa.  
39  
40  
41  
42  
43  
44  
45  
46  
47  
48  
49  
50  
51  
52  
53  
54  
55  
56  
57  
58  
59  
60  
61  
62  
63  
64  
65

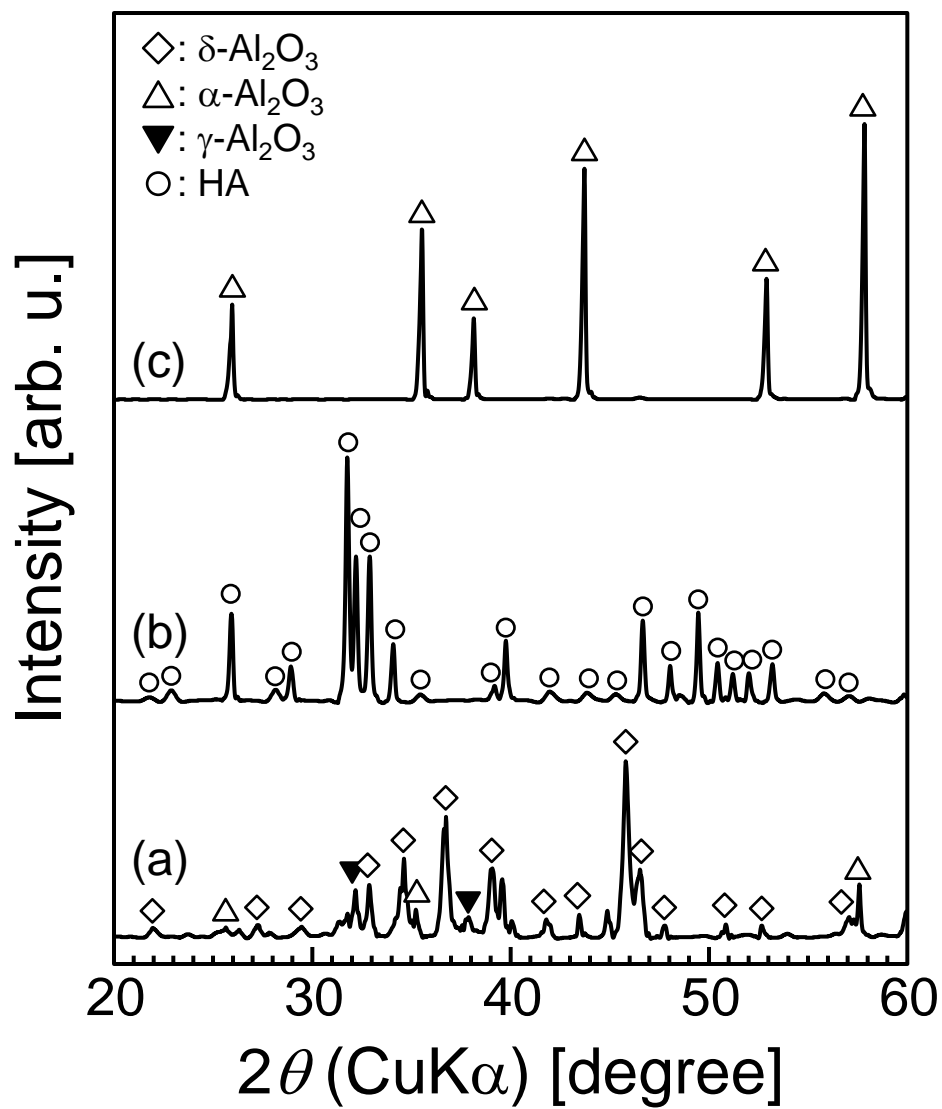


Fig. 1 M. Kawashita *et al.*

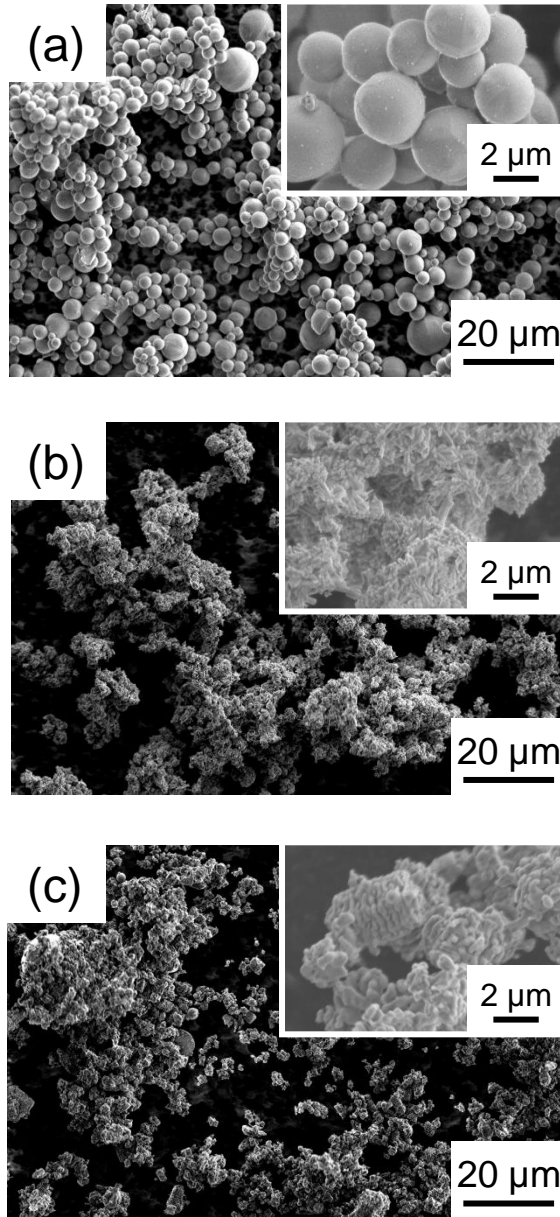


Fig. 2 M. Kawashita *et al.*



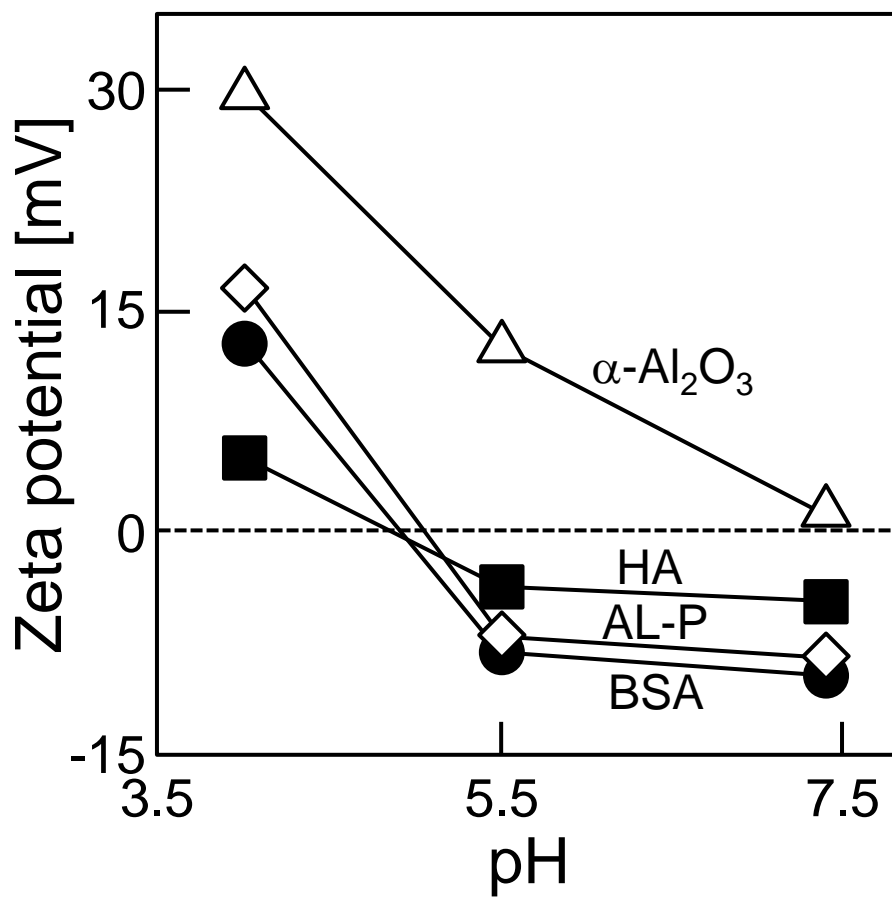


Fig. 3 M. Kawashita *et al.*

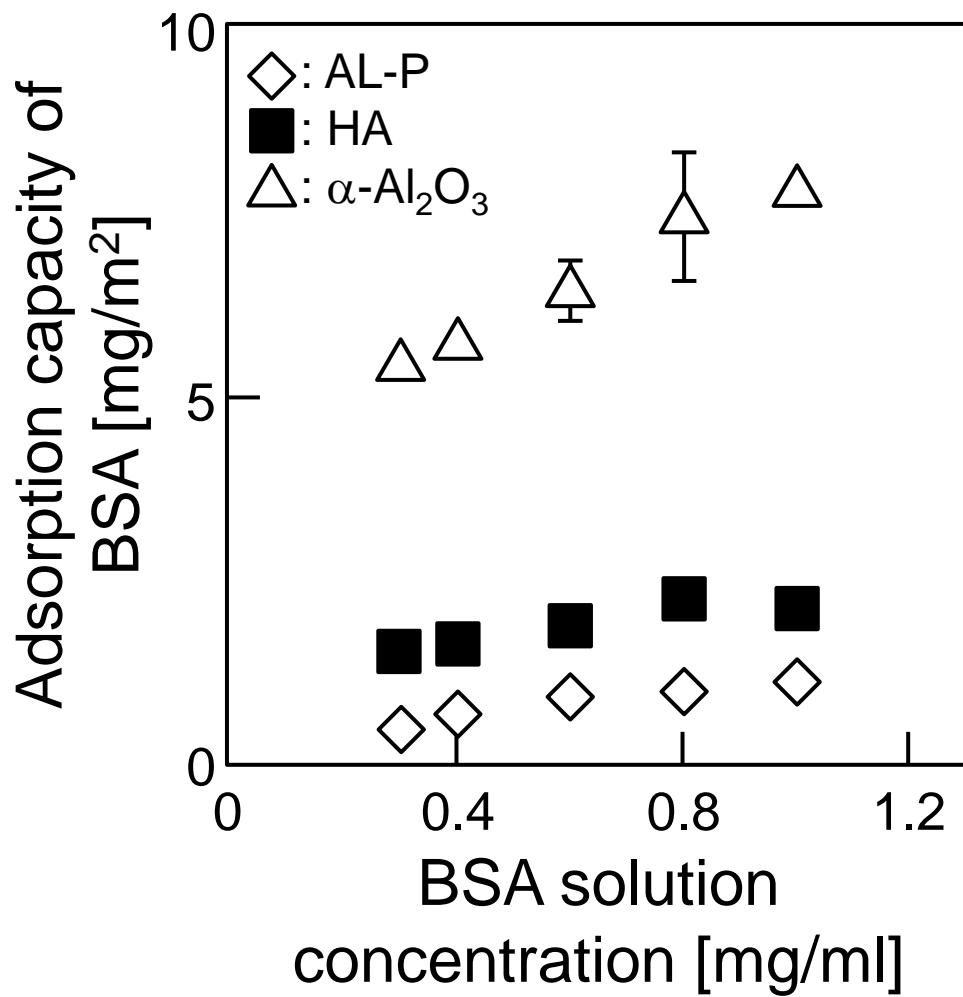


Fig. 4 M. Kawashita *et al.*

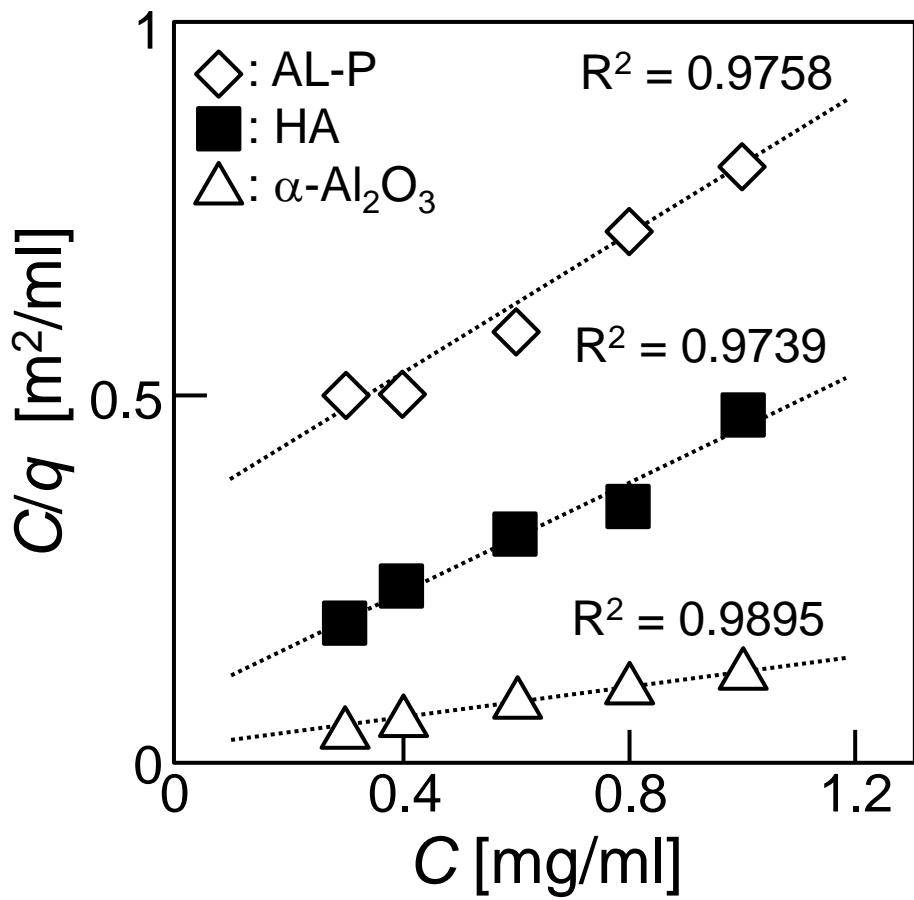


Fig. 5 M. Kawashita *et al.*

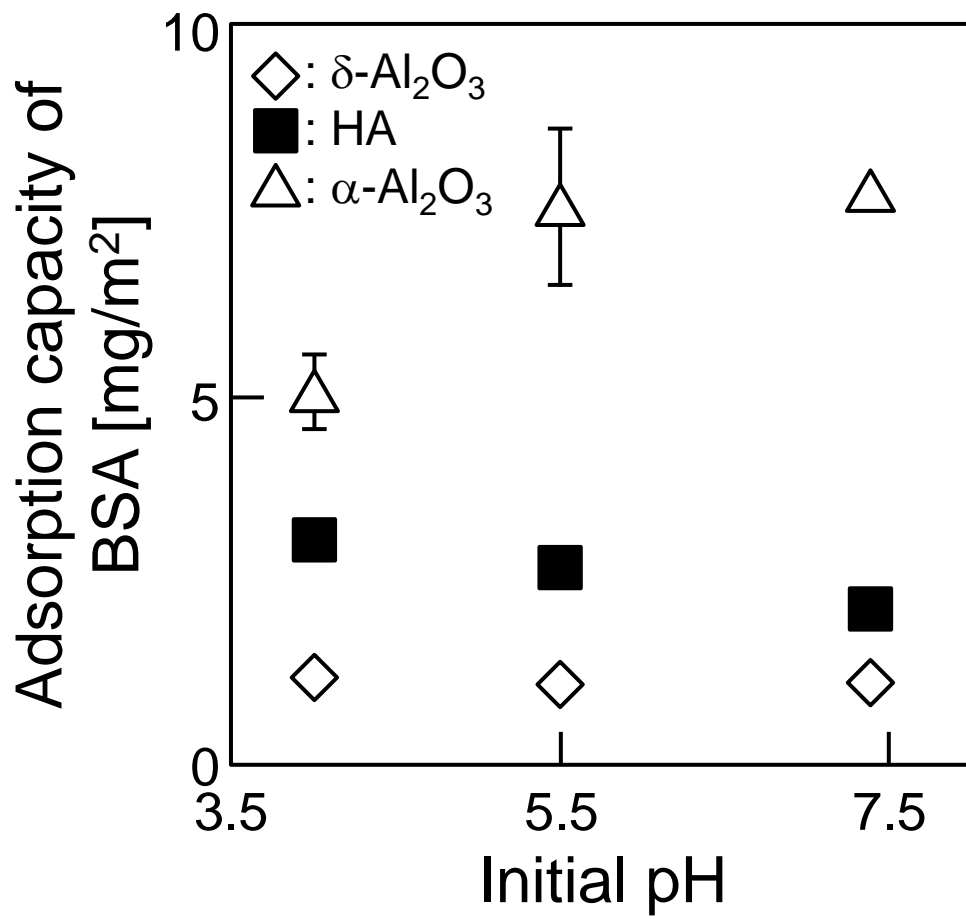


Fig. 6 M. Kawashita *et al.*

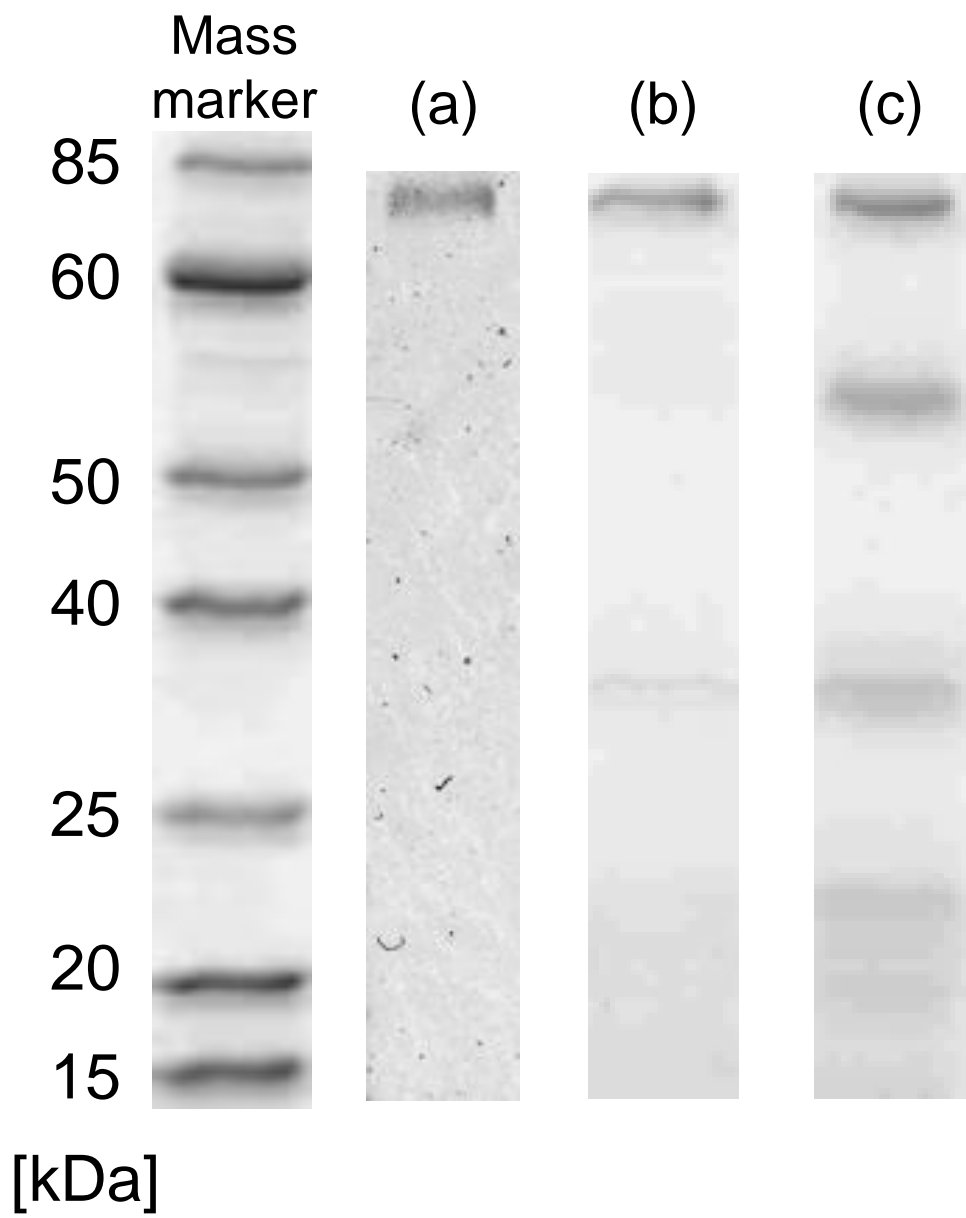


Fig. 7 M. Kawashita *et al.*

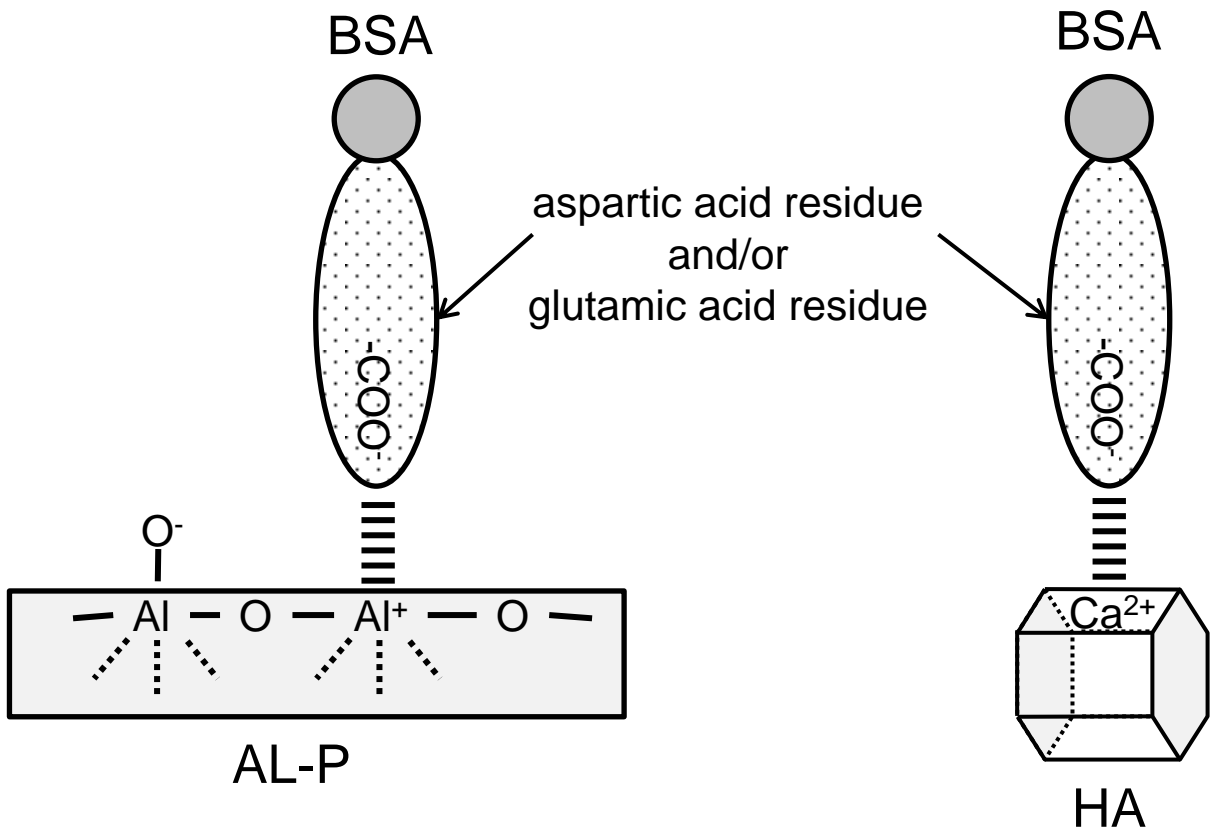


Fig. 8 M. Kawashita *et al.*

Table 1 Candidates of BSA fragments with mass of molecular around 35 and 55 kDa

Amino-terminal domain (position)	Carboxyl-terminal domain (position)	Mass of molecular [kDa]
K (64)	K (545)	55.1
K (4)	R (485)	55.0
K (93)	K (574)	55.0
K (20)	K (500)	54.7
K (41)	K (521)	54.7
R (10)	K (317)	35.0
K (93)	K (397)	35.0
K (128)	K (432)	35.0
R (197)	K (505)	35.0
R (218)	K (525)	35.0